Hydrol. Earth Syst. Sci. Discuss., doi:10.5194/hess-2016-689, 2017
Manuscript under review for journal Hydrol. Earth Syst. Sci.
Published: 9 January 2017

Hydrology and Earth System Sciences
Open Access
Discussions

Sub catchment Assessment of snowpack and snowmelt change by analyzing elevation bands and parameter sensitivity in the high Himalayas

Vishal Singh[1], Manish Kumar Goyal[1], Rao Y. Surampalli[2], and Francisco Munoz-Arriola[3,4]

[1]Department of Civil Engineering, Indian Institute of Technology, Guwahati-781039, India

[2]Global Institute for Energy, Environment, and Sustainability, P.O. Box 14354, Lenexa, Kansas 66285, USA

[3]Department of Biological Systems Engineering, University of Nebraska-Lincoln, USA

[4]School of Natural Resources, University of Nebraska-Lincoln, USA

Keywords: Hydrological modeling, Himalayas, SWAT and SWATCUP, Snowpack and snowmelt, elevation bands.

Correspondence to: Francisco Munoz-Arriola (fmunoz@unl.edu)

Abstract: The present work proposes to improve estimates of how much streamflow is generated by snow in the watersheds of the steep Himalayas. Half of the earth's glacial catchments in nonpolar areas are in the Himalayas, and they generate almost a third of the streamflows in India. In River catchments with glacier presence in the region, temporal variability in streamflow generation and the associated distribution of accumulated snow illustrate how changes in snowmelt and precipitation can affect water supplies to a growing population of 1.3 billion people. Estimations of snowpack and snowmelt in watersheds are critical for understanding streamflow generation and sources of catchments. However, estimating precipitation and snow accumulation is constrained by the difficulties complex terrain poses to data collection. The primary objective of this study is to assess the role of elevations in the computation of snowfall (snowpack) and snowmelt in sub-catchments. The study area is the Satluj River Catchment (up to Kasol gauge) with moderate (e.g., 526 m) to very high elevations (e.g., 7429 m) dominated by snow covers and glaciers. The Satluj River Catchment was divided into 14 sub-catchments. Snowpack and snowmelt variations in the sub-catchments in both historical and projected near-term (2011-2130) periods were analyzed using observed and Global Circulation Model (GCM) data sets. Both hydrological scenarios used elevation bands and parameter-sensitivity analyses built in the Soil Water Assessment Tool (SWAT) model. For model calibration/validation and parameter sensitivity analysis, an advanced optimization method—namely, Sequential Uncertainty Fitting (SUFI2) approach was used with multiple hydrological parameters. Among all parameters, the curve number (CN2) was found significantly sensitive for computations. The snowmelt hydrological parameters such as snowmelt factor maximum (SMFMX) and snow coverage (SNO50COV) significantly affected objective functions such as R^2 and NSE during the model optimization process. The computed snowpack and snowmelt were found highly variable over the Himalayan sub-catchments as also reported by previous researchers in other regions. The magnitude of

Hydrol. Earth Syst. Sci. Discuss., doi:10.5194/hess-2016-689, 2017
Manuscript under review for journal Hydrol. Earth Syst. Sci.
Published: 9 January 2017

Hydrology and Earth System Sciences
Discussions

snowpack change consistently decreases across all the sub-catchments of the Satluj River Catchment (varying between 4% and 42%). The highest percentage of changes in snowpack was observed over high-elevation subcatchments.

1. Introduction

Most of the perennial river channels such as the Ganga, Indus, and Brahmaputra are originated in Himalayan glaciers. Large snowpacks along the Himalayas are formed by thousands of glaciers in valleys and are the major sources of fresh water reserves in India (Bolch et al., 2012). Many studies reported that the hydroclimatology of the Himalayan catchments is changing, and thus snowpack and glaciers are reducing their mass, which leads to more snowmelt water into the streams (Bhambri and Bolch, 2009; Bolch et al., 2012; Xu et al., 2016; Singh et al., 2016). According to the Intergovernmental Panel on Climate Change (IPCC, 2013), changes in temperature and precipitation are expected to affect the hydrology of Himalayan catchments (IPCC, 2013). Some of these changes can be reflected in the spatial distribution and temporal variability of rainfall, snowfall and glaciers' mass, which at the same time can drive streamflow generation in large catchments in the Himalayas (Singh et al., 2008). While glaciers influence streamflows in high altitudes, rainfall is considered a predominant factor in low altitudes. As a main tributary of the Indus River, the Satluj River has its flow primarily generated by snowmelt during the spring. Thus, a higher melting will result in an increase in runoff downstream before the monsoon season (Jain et al., 2010) and increased vulnerability to floods and risk to the sustainability of agriculture in the Punjab region. Other areas of the world, such as the western United States of America, have experienced increments in altitude of snow accumulation reduction of the snowpack, and earlier snowmelt onsets (Motte et al., 2005; Mote, 2006). All of these factors influence water supply and storage and affect the sustainability of human activities downstream. However, in the Sutlej River Catchment, recent and projected changes in snowmelt and snowpack are inconclusive about how glacial and perennial streamflow will be affected in a changing climate.

Several studies highlighted an elevation-dependent warming and revealed that changes in temperature lapse rate (TLR) and precipitation lapse rate (PLR), due to climate change, are responsible for the higher reduction in the snowpack at high elevations than those present at lower elevations (Singh and Goyal, 2016a; Singh and Goyal, 2016b). The TLR and PLR are functions of elevation (Gardner et al., 2009), and thus the snowpack and snowmelt rate can be affected by variations in TLR and PLR as analyzed by Singh and Goyal (2016a and 2016b) over eastern Himalayan catchments. After temperature, alterations in precipitation pattern have been recognized as another major factor that determines changes in snowpack over the region. Thus, climate change projections indicate an increment in precipitation variability (Change, I.C., 2013) which will influence PLRs (Singh and Goyal, 2016a) and snowfall patterns, particularly when catchments' topography corresponds with moderate to very high elevations like the Himalayas. Also, influences of a changing climate in the Himalayan regions have evidenced long-term shifts in average air temperature, precipitation and other land surface variables (Sridhar and Nayak, 2010; Jain et al., 2010;

Hydrol. Earth Syst. Sci. Discuss., doi:10.5194/hess-2016-689, 2017
Manuscript under review for journal Hydrol. Earth Syst. Sci.
Published: 9 January 2017

Hydrology and Earth System Sciences
Discussions

Beniston, 2012; Narsimlu et al., 2013;). Bolch et al. (2012) reported that the length of many Himalayan glaciers is shortening, and only 25% of glaciers are stable. Therefore, future changes, especially near-term changes, have made it increasingly important to be able to compute snowpack and snowmelt in sub-catchments to manage water resources.

Several studies successfully used the SWAT model to project water yield and streamflow as a function of the variable temperature and precipitation using Coupled Model Intercomparison Project Phase 3 (CMIP3 or CM3) Global Circulation Model (GCM) data sets (Ferrant et al., 2014; Shrestha et al., 2013). Neupane et al. (2014) used SWAT to simulate the effect of climate change on natural water storage at watersheds, evidencing the influence of precipitation and temperature lapse rates and inherent snow accumulation and snowmelt roles. Glacial hydrologic assessments can help track and predict water availability in catchments reliant on snowpack and timing snowmelt. The primary objective of this study is to show the scope of computation and characterization of snowpack and snowmelt in sub-catchments, which could help in understanding modeling complexities, mainly snowmelt induced in the Satluj River catchment. Another important objective of this study is to highlight the near-term future changes in snowfall and snowmelt using GCMs.

2. Methodology

2.1. Study area

The Satluj River Catchment is a part of the Indus River system, which has many major tributaries--such as the Satluj, Beas, Jhelum, Chenab and Ravi--and minor tributaries. The current research focused on a part of the Satluj River Catchment (up to Kasol gauge station), which stream flows through the western Himalayan region. The main outlet point, Kasol, consists of an area about 51055 km^2, which is located at the head of the Bhakra Dam of India. The geographical extent of the study area lies between 77°00’ to 82°39’ E longitudes and 30°8’ to 33°00’ N latitudes (Fig. 1). The Satluj River is the longest river among the five major rivers that flow through northern India and Pakistan. It is north of the Vindhya Range, south of the Hindu Kush segment of the Himalayas, and east of the Central Sulaiman Range in Pakistan. The Satluj Catchment is mainly covered by snow. Glaciers of the Satluj River are at moderate (526 m) to very high elevations (7429 m). The majority of the Satluj River catchment is fed by snowmelt (up to the Rampur gauge station) and rainfall during the summer and by groundwater flow during the winter.

2.2 Historical and near-term scenarios

Daily precipitation, minimum and maximum temperature, humidity, wind speed and solar radiation were obtained from the Indian Meteorological Department (IMD) and Indian Institute of Tropical Meteorology (IITM), Pune, India, in grid format (at $1^\circ \times 1^\circ$ scale). Six grids with all of these variables were kept for the drainage area of the Satluj catchment for the historical time series (1991-2008). Additionally, three gauge locations with daily measured precipitation were also used for the same time duration. The geospatial thematic data layers such as SRTM (Shuttle Radar Topographic Mission) digital elevation model (DEM) with 90 m spatial resolution (GLCF, 2005) and landuse/landcover (LULC) map (prepared at 1:50,000 topographical scale using IRSP6 LISS III satellite data sets) were used in the study. The description of the LULC codes is given in the SWAT user manual written by Neitsch et al. (2011). A soil map of India (Figure 1) downloaded from SWAT portal (www.swat.tamu.edu/conferences/international/2012/data set/) was also used (FAO, 2007). The description of soil categories came from FAO's world harmonic soil database (FAO, 2007).

For the assessment of near-term (2011 to 2030) snowpack, snowmelt and water yield, daily precipitation and temperature data sets were downloaded from the IPCC climate data portal. CGCM3.1/T63 atmospheric and sea-ice model outputs–namely, SRES B2 model experiment (Qiao et al., 2013)--were used. CMIP3-SRES B2's daily temperature and precipitation were provided at 128x64 Gaussian grid (approximately 2.81° latitudes x 2.81° longitudes) (Thornton et al., 2009) and bias corrected (Taylor et al., 2012; Mahmood and Babel, 2012; Singh and Goyal, 2016b;). The SRES B2 model experiment was selected for the near-term assessment based on the comparison of IPCC's SRES B1, SRES A2, 20C3M, COMMIT and B2 historical simulations and observed precipitation and temperature. Four GCM data points which fell in the current study area and highlighted the spatial variations of the present study were considered without downscaling (Fig. 1). The occurrence of snowpack and snowmelt changes due to variations in elevation bands is enhanced by dividing the main catchment into sub-catchments. For the sub-catchment calculations, observed grids (six), gauge data sets (3 points) and GCM data grids (four) were spatially interpolated at each sub-catchment using the Inverse Distance Weighting Approach (IDWA) (Lu and Wong, 2008; Snell, 1998, Snell et al., 2000).

2.3. Spatiotemporal approach

Up to 10 elevation bands were incorporated in each sub-catchment to characterize the snowpack and snowmelt. For this, at each subcatchment scale, an average TLR and PLR were computed and incorporated into the SWAT model to improve the snowmelt and snowpack computations. The present study uses a stochastic procedure SUFI2 to characterize model uncertainty and sensitivity analyses to improve modeling outputs in a snow-glacier dominant Himalayan catchment. The model calibration and validation were done using daily measured discharge data at three gauges: Rampur, Suni and Kasol. Hydro-meteorological observations, especially daily measured discharge data from 1989 to 2008 at all three gauges, were used to improve the modeling in both historical (1991-2008) and near-term projection scenarios (2011-2030). The historical scenarios of snowpack, snowmelt and other water balance components were generated using hydro-meteorological data from 1991 to 2008. Near-term scenarios used two of the most relevant GCM variables, temperature and precipitation, to produce the snowfall and snowmelt. CM3 GCM model's daily temperature and precipitation were used to analyze the near-term complexities and changes in snowpack and snowmelt (Ferrant et al., 2014; Shrestha et al., 2013).

The Satluj River Catchment was divided into 16 sub-catchments based on the area threshold method (Ficklin and Barnhart, 2014; Neitsch et al., 2011). Each sub-catchment includes a main channel and multiple HRUs which

Hydrol. Earth Syst. Sci. Discuss., doi:10.5194/hess-2016-689, 2017
Manuscript under review for journal Hydrol. Earth Syst. Sci.
Published: 9 January 2017

consist of geospatial representations of homogeneous land use, soil type, and management practices. The contributions of each HRU were weight-averaged for every sub-catchment (Zhou et al., 2014). Simulated snowpack and snowmelt were computed at each HRU and also aggregated by sub-catchment. For each sub-catchment, up to 10 elevation bands were defined; then, at each elevation band, all snow hydrological parameters were determined (Neitsch et al., 2011). To estimate the spatial variability of the snowpack and snowmelt, an average TLR and PLR were incorporated at each sub-catchment, which adjusted the temperature at each elevation band. Snow and glaciers mainly cover the upper part of the catchment that has a very low TLR, while the lower part of the catchment has a reduced presence of glacier areas with large settlements and high temperatures. These topographical variations brought high variability in TLR and PLR over the Satluj River catchment. The rationale for discretizing the catchment is to simulate streamflow, snowfall and snowmelt processes at each sub-catchment and the respective elevation bands, which is also contributes to account homogeneous land use, soil, and weather generator parameters (e.g., precipitation and temperature). A representation of the water balance components at each sub-catchment, elevation band, and HRUs could be useful to highlight the catchments' variability in an efficient manner especially in the case of large-area catchments.

2.3.1. Modeling approach

The SWAT model is fully capable of computing the long-term water balance components in a semi-distributed manner through the use of hydrological response units (HRUs). Streamflow is simulated using a slope-adjusted modified Soil Conservation Services curve number (CN) method (USDA Soil Conservation Service, 1972; Arnold et al., 1998). Detailed physical and hydrological principles and parameters are fully described in the SWAT user manual (Neitsch et al. 2011).

2.3.2. Model calibration and validation

Simulated and observed streamflows were used in a SWAT stochastic optimization tool, Calibration and Uncertainty Program (CUP), to calibrate and validate physical parameters (Abbaspour et al., 2007). Recorded daily streamflows at three outlet locations (i.e., Rampur, Suni and Kasol) for the period of 1989 to 2008 were used. The initial two years were considered a warm-up period for the historical scenario, and the initial three years for the near-term projected scenarios. The model calibration was performed using the concept of aggregate parameter selection (Yang et al., 2007). An 'aggregate parameter' is obtained by adding terms such as v_, a_ and r_ to the front of the original parameter to create an absolute increase and a relative change in the initial parameter values, respectively (Zhang et al., 2014). The objective functions such as coefficient of determination (R^2) and Nash-Sutcliffe Efficiency Index (NSE) were used in the calibration and validation procedures (Abbaspour et al., 2007; Zhang et al., 2014).

2.4. Sensitivity analysis

Model outputs are deterministic representations of precipitation, discharge, evapotranspiration (ET), storage and different transport-processes' variables and state variables. A deterministic hydrological model such as SWAT is unable to explore the stochastic behavior of random variables such as rainfall and associated discharges (Abbaspour et al., 2007; Singh et al., 2013). Calibration of any distributed hydrological model using observed hydro-observation data sets always leads to nonidentifiable parametric uncertainties due to complex hydrological processes and data sets, especially in the case of the large catchments (Yang et al., 2007). Thus, it's necessary to estimate the propagation of parameter uncertainty to the uncertainty of the model's outputs. SWAT uses an independent stochastic model SUFI2, which in this work is selected to account for model uncertainty (Yang et al., 2007; Abbaspour et al., 2007).

SUFI2 accounts for parametric uncertainty through sequential and fitting approaches. Iteratively old coefficient parameters are updated into a new array of coefficients during calibration to ultimately achieve the final set of parameters (Abbaspour et al. 2011). The SUFI2 algorithm assumes a large parameter uncertainty (or physically meaningful range) occurring in response to data inputs to ensure the observed data fall into the 95% prediction uncertainty (95PPU) band during the first iteration. During this iterative procedure, uncertainty progressive decrease is monitored though the changes of the p-factor and r-factor (Abbaspour et al., 2007). While the p-factor determines the percentage of simulated data falling into the observed-data range, the r-factor contributes to determine the uncertainty of the simulated variables and state variables when compared with observed data sets.

The value of the p-factor ranges between 0 and 100%, and the r-factor ranges between 0 and infinity. A value of p-factor = 1 and r-factor = 0 represents a perfect match between simulated and observed data. The parameter sensitivity analysis helps identify the significance of a particular parameter to the calibration process, whether the process is influenced by the parameter values or nature of the forcings. SUFI2 method is based on a global sensitivity analysis (GSA) performed through multiple regression. GSA's parameters were generated through a Latin hypercube sampling (LHS) and the resultant simulated variables and state variables are contrasted to the equivalent observations through the application of an objective function. The LHS method is considered a highly efficient sampling method; it can reduce the sampling points within an individual space. In this study, four iterations with 600 simulations were conducted to estimate the uncertain effect of model parameters in the calibration outcomes.

In general, after completion of the first iteration, the model performed well using the majority of parameter combinations sampled from the updated parameter ranges. Therefore, the updated parameter ranges used during the second iteration are regarded as the uncertainty ranges for model simulations and analyses. In this study, the statistical significance tests such as p-value test and t-stat were employed to rank parameters from high sensitive to nonsensitive. A 0 p-values shows a highly sensitive parameter in the GSA . On the other hand, GSA's t-stat is evaluated based on the significance level alpha ($\alpha = 0.05$) and resultant p-values. The alpha value 0.05 was chosen as the local significance level. Based on this significance level, values larger than +1.96 indicate a significant ($p<0.05$) positive sensitivity and values lower than -1.96 indicate a significant ($p<0.05$) negative sensitivity. Thus, the p-values closer to zero will enable the use of trend analyses of the simulated variables and state variables (Abbaspour et al., 2011). The parameter-sensitivity results can be observed in Table 3.

2.5. Elevation band approach for snowpack and snowmelt measurement

In this study, SWAT snowmelt hydrology and related processes were performed at the sub-catchment scale (Fontaine et al., 2002). Therefore, each sub-catchment was divided into 10 elevation bands in order to incorporate temperature and precipitation variations with respect to altitude (Neitsch et al., 2011). The sequence of methodological steps are as follows:

2.5.1. TLR and PLR computation and their adjustments at each elevation band

For each sub-catchment, lapse rates for precipitation p_{laps} (mm/km) and temperature t_{laps} (ºC/km) were computed as Eq. 1:

$$\boldsymbol{P_B = P + (Z_B - Z)\frac{p_{laps}}{days_{pcp,yr} \times 1000}} \quad \text{and} \quad \boldsymbol{T_B = T + (\ Z_B - Z)\frac{t_{laps}}{1000}} \tag{1}$$

where P (mm), T (ºC) and Z (m) were the sub-catchment precipitation, temperature and recording gauge elevation, respectively; while $\boldsymbol{P_B}$, $\boldsymbol{T_B}$ and $\boldsymbol{Z_B}$ were the adjusted precipitation, temperature and mean elevation for each elevation band. The variable $days_{pcp,\ yr}$ represented the mean annual number of days with precipitation. The temperature lapse rate could be computed using mean annual temperature. In accordance with the delineation approach used with sub-catchments, temperatures were adjusted within each elevation band by comparing the elevation bands' midpoint elevation ($\boldsymbol{Z_B}$) within the station elevation (Z). The elevation difference was multiplied by the lapse rate to calculate a temperature difference between the station elevation and the elevation band. An updated elevation band mean temperature ($\boldsymbol{T_B}$) was calculated by adding or subtracting the temperature difference to or from the temperature measured at the station elevation (T) as in Eq. 2:

$$\boldsymbol{T_B = T + (Z_B - Z)\frac{dT}{dZ}} \tag{2}$$

where $\boldsymbol{\frac{dT}{dZ}}$ is the mean local lapse rate ($\boldsymbol{t_{laps}}$)(ºC/km) calculated at all sub-catchments. A lapse rate for annual precipitation was represented by the changes of the mean annual precipitation with respect to the station elevation. Adjusted precipitation in each elevation band ($\boldsymbol{P_B}$) was based on the difference between the elevations of the subcatchment meteorological station (Z) and each elevation band ($\boldsymbol{Z_B}$) multiplied by the lapse rate of (mm/km) per event (P). If the meteorological station was unavailable in a particular subwatershed, then the next nearest meteorological station was considered for lapse rate calculations. The equation was defined as Eq. 3:

$$\boldsymbol{P_B = P + (Z_B - Z)\frac{dP}{dZ}} \tag{3}$$

where $\boldsymbol{\frac{dP}{dZ}}$ was the mean local lapse rate ($\boldsymbol{p_{laps}}$) calculated for all sub-catchments.

2.5.2 Snow Accumulation

The snowpack was represented in SWAT by the snow water equivalent (the mass of liquid water in the snowpack) SWE (mm), which balanced snowfall SF (mm) and snowmelt SM (mm) or sublimation ES (mm) (Eq. 4):

Hydrol. Earth Syst. Sci. Discuss., doi:10.5194/hess-2016-689, 2017
Manuscript under review for journal Hydrol. Earth Syst. Sci.
Published: 9 January 2017

Hydrology and Earth System Sciences
Discussions

$$SWE_{day} = SWE_{(day-1)} + SF - SM - E_s \tag{4}$$

In SWAT, snowmelt *SM* is controlled by the air and snowpack temperatures, the melting rate, and areal coverage of snow. When daily mean air temperature is less than a snowfall temperature, as specified by the SWAT variable SFTMP (Table 1), the precipitation within an HRU is classified as snow, and the liquid water equivalent is added to the already-present snowpack. The snowpack temperature is a function of the mean daily temperature during the preceding days and varies as a dampened function of air temperature (Anderson, 1976). The influence of the previous day's snowpack temperature on the current day's snowpack temperature was controlled by a lagging factor, (*TIMP)*, which intrinsically accounts for snowpack density, snowpack depth, exposure and other factors known to affect snowpack temperature (Eq. 5):

$$T_{snowpack(day)} = T_{snowpack(day-1)} \times (1 - TIMP) + T_{av} TIMP \tag{5}$$

where $T_{snowpack}$ (day) and $T_{snowpack}$ (day-1) are the snowpack temperature (*℃*) on a given day and on the day preceding it, respectively, and T_{av} (*℃*) is the mean air temperature for the same given day. The fraction of area covered by snow SNO_{cov} can be computed as Eq. 6:

$$sno_{cov} = \frac{SNO}{SNO_{100}} \left(\frac{SNO}{SNO_{100}} + exp\left(cov_1 - cov_2 \frac{SNO}{SNO_{100}} \right) \right) - 1 \tag{6}$$

where *SNO* is the water content of the snow pack on a given day (mm), SNO_{100} is the threshold depth of snow at 100% coverage (mm), and cov_1 and cov_2 are coefficients that define the shape of the curve. Snow depth over an elevation band is assumed to be constant when the *SWE* exceeds SNO_{100}; i.e., the areal depletion curve affects snowmelt only when the snowpack water content is between zero and SNO_{100}.

2.5.3. Snowmelt and glacier melt

Snowmelt rate is controlled by snowpack temperature and air temperature. A snowpack cannot begin to melt and release water before the entire pack has reached 0°C and thus we adopted the same. The SWAT model is unable to calculate glacier melt contributions directly. It corresponds to snowmelt contribution mainly from the snowpack amount. Hence, in this study the snowmelt amount integrated glacier melt and snowmelt. The melt rate from a snowpack varies in response to snowpack conditions (Fontaine et al., 2002). In this study, snowmelt and glacier melt were set up together in the SWAT model as a linear function of the difference between the average of the snowpack and glacier temperature ($T_{snowpack}$) and the maximum air temperature (T_{max}) on a given day and the base or threshold temperature for the snowmelt (Eq. 7). It is worth stating that due to the large number of glaciers over the Satluj catchment, the temporal mass balance of glaciers and melting rates were analyzed at the catchment and HRU levels, respectively. Hence, standard coefficient values were used:

$$SM = b_{mlt} \times sno_{cov} \left[\frac{T_{snowpack} + T_{melt}}{2} - TMLT \right] \tag{7}$$

where b_{mlt} (mmH_2O/day-°C), is the melt factor for a day:

$$b_{mlt} = \frac{SMFMN+SMFMX}{2} + \frac{SMFMN-SMFMX}{2} sin\left(\frac{2\pi}{365}(d_n - 81)\right) \quad (8)$$

Eq. 8 has been adapted for application in the Northern Hemisphere, where *SMFMN* is the melt factor for 21st June, *SMFMX* is the melt factor for 21st December, and d_n represents the day of the year.

3. Result and analysis

Geophysical components, such as topography, land use/land cover change and soil classes, are parameterized in SWAT (Neitsch et al., 2011) and help determine the spatial distribution of water availability and its physical-state. For example, more than 30 different soil parameters associated with each soil category such as soil texture, available water content, hydraulic conductivity, bulk density and organic carbon content were used for this study. These parameters in SWAT were defined for each soil subtype for different layers (between two and three layers). A key parameter in SWAT, the curve number (CN) averaged 80.1 in the catchment, though it varied from lower subcatchment to upstream subcatchment as per LULC, slope and soil properties.

SWAT information on model implementation, including the temporal context for the simulated water balance components for the sensitivity analyses is described in Table 1. The sensitivity results were a product of 20 different hydrological parameters (Table 2) on both daily and monthly time steps. In Table 3, the parameters which were found sensitive to snowmelt-induced streamflows are selected for model calibration. The description of parameters and their coefficients are given in Table 3. For example, TLAPS.sub parameter (TLR) fluctuates from -7.0 ˚C/km to 2.5˚C/km (with the best-fitted value computed as -4.1 ˚C/km), showing how temperature variations exist across the Satluj River Catchment. Table 3 also shows the aggregate parameter ranges that result from the final iteration number, which was optimized through the Latin Hypercube Sampling (LHS) method (Abbaspour et al., 2011). For TLAPS.sub, the p-value is recorded as 0.01 and its t-stat value is recorded as -2.2, also illustrating that this parameter is found sensitive for the model calibration and validation.

Among the 20 calibration parameters, the 5 parameters R_CN2.mgt, R_SMFMX.bsn, V_CH_K2.rte, TLAPS.sub and V_GW_DELAY were computed as significantly sensitive parameters for daily calibration while the parameters SNO50COV.bsn, CN2.mgt, GW_DELAY.gw and SOL_K.sol were found sensitive for monthly analysis. The computed t-stat values were less than -1.96 or greater than +1.96; the estimated p-values were close to zero. At daily time steps, sensitive parameters evidence the role of snow melt and the temperature lapse rate on water flowing in the model. Further, soil properties also evidence the regulatory role of infiltration in the subsurface. For example, the V_GW_DELAY.gw parameter of aquifer recharge at the catchment was found significantly sensitive for both daily and monthly time steps (Table 3). In unconfined and shallow aquifers, this factor could influence the temporal variability and spatial distribution of different components of the water balance, highlighting the contributions of surface water and groundwater interactions. Also, at the catchment scale A_ALFA_BF.gw, whose p-value was recorded as 0.172 daily and 0.406 monthly, was found insignificant for the model calibration, indicating the sensitivity of the model's baseflow parameterization.

Other model parameters associated with different types of LULC and soil categories were not found sensitive for the model calibration and validation process. These model parameters included GWQMN.gw, HRU_SLP.hru, SOL_BD.sol, HRU_SLP, PLAPS.sub, CH_N2.rte, SOL_AWC.sol and GW_REVAP. The snowmelt temperature-related parameters such as R_SMTMP.bsn, R_SFTMP.bsn and R_SMTMP.bsn were also recorded nonsignificant during model calibration as shown in Table 3. These properties are relevant to the temperatures that allow the formation or accumulation of snow, rather than the melting of snow already packed (which coincides with the sensitivity of the SMFMX parameter described above). The Saltuj River drainage area is dominated by glacial hydrology, permanent ice sheets and seasonal well-packed snow. These, are typical features of the catchment, which at the same time are identified in the sensitivity of parameters such as R__SNOCOVMX.bsn and SNO50COV.bsn (parameters that represent the fraction of snowpack and the elevation bands) and the recorded significant parameter sensitivity of daily and monthly calibration, respectively. The significance of elevation differences is reflected in the snowpack computations. The curve number coefficient (R_CN2) was the most significantly sensitive parameter in the model calibration process. CNs were modified based on the fractional HRU slopes so soil physical properties could vary at sub-catchment scale. Thus, groundwater delays and baseflow, together with management practices, soil physical properties (i.e., the CN), and snow properties, influence the generation of return flows, which aligns with the purpose of this work in the Satluj River Catchment.

Table 4 presents the daily and monthly results for streamflow calibration (1991 to 2000) and validation (2001 to 2008) at all three outlet locations, Rampur, Suni and Kasol. Table 4 also shows the goodness-of-fit between the simulated and measured streamflows with the coefficient of determination (R2) and Nash-Sutcliffe Equation (NSE) (Legates et al., 1999) for the Rampur, Kasol and Suni outlet stations. The computed R2 and NSE are found reasonably acceptable for daily and monthly observations. Regarding goodness-of-fit aspects, monthly and daily calibration correlations were similar. Among all the three outlet stations, Kasol and Rampur show better calibration and validation statistics than does Suni station. Before initialization of the model calibration, we took 5% as bias to ignore the extreme ambiguities from the calibration.

Uncertainty results, which were computed using the objective functions p-factor and r-factor, provide insights about the precision and accuracy of model simulations (Abbaspour et al., 2011). Also, factors refer to the final uncertainty level of the calibration-validation approach. The p-factor values recorded during model calibration for the Rampur, Kasol and Suni stations were 0.46, 0.57, and 0.52 daily and 0.41, 0.57, and 0.49 monthly for the timespan 1991-2000 (Table 4). During model validation, the p-factor values recorded were 0.43, 0.52, and 0.53 dailyand 0.45, 0.60 and 0.58 monthly. Along the Satluj River Catchment, resultant p-factors indicate that more than 50% of the simulated flows were encompassed within the uncertainty bonds for Kasol station's daily and monthly simulations, as well as for calibration and validation approaches. In contrast, simulated flows for Rampur showed p-factors below 50%, contrasting with their performance on the SWAT model for Kasol and Suni stations during daily simulations and for model validation. On the other hand, the r-factor values recorded were 1.89, 1.50, and 1.60 daily and 1.90, 1.57, and1.43 monthly for Rampur, Kasol and Suni. During model validation, the r-factor values were calculated as 1.89, 1.67, and 1.72 daily and 1.92, 1.62 and 1.52 monthly for Rampur, Kasol and Suni. Resultant r-factors indicated the SWAT's ability to precisely reproduce flow values; however, values above 1.43 indicated that other sources of error besides model physics could contribute to the values of the r-factor. The experiments described here are unable to identify the contribution of such sources of error. Kasol, Suni, and Rampur were the only stations with observed data and all were located in the lowest drainage area in the Sultej River Catchment. Although small, differences among model performance metrics illustrate the local contributions of Suni and Rampur's downstream drainage areas to the total streamflow generated at Kasol. Kasol "averages" over and under estimations of streamflows generated upstream, so lower r-factor values are expected, representing higher precision. Further, smaller values of p-factor in Kasol also indicate a lower accuracy of the model in replicating observed streamflows within the uncertainty bonds.

Considering that most of the drainage areas of this catchment are snowmelt-dependent and are upstream of Rampur station, a deeper assessment of snowfall and snowmelt along with streamflow generation is required at high altitudes. The temporal variability and spatial distribution of the hydrological components such as precipitation, snowpack, snowmelt, water yield (contributed by rainfall only) and total water yield (contributed by both snowmelt and rainfall) were computed and analyzed. Figure 2 illustrates the aggregation of simulated snowpack and snowmelt compared with precipitation from 1991 to 2008 in sub-catchments. Here, it is evident that the maximum snowpack contribution occurs at sub-catchments at a high elevation. These sub-catchments, such as SB1, SB2, SB3, SB4, SB15 and SB16, have values varying from ~10 to ~380 mm in a single year. Figure 2 also shows that sub-catchments such as SB10, SB11, SB12, and SB13, located in the lowest drainage areas, poorly contribute to the snowpack of the Saltej River Catchment. (They had annual values below 150 mm predominantly). Interannual changes in snowpack and the amount precipitation show local to large-scale influences in snow melt as well as snow accumulation. For example, SB1 shows that the proportion of snowmelt/snowpack with respect to precipitation was larger in 2000 and 2002, which contrasts with those proportions between 1995 and 1996. In the easternmost portion of the catchment, this proportion is consistent during all years, which contrasts with the catchment's lower drainage areas. Further analysis is required to identify causality in those accumulations in response to El Niño Southern Oscillation or interannual changes in monsoon intensity and interannual accumulation of snow. Figure 3 illustrates a possible influence of elevation differences along the catchment.

During near-term projection, input parameters such as DEM, LULC, and soil map were kept constant to simulate and isolate possible effects of temperature and precipitation, which could emerge in places with highly variable elevations and large elevation gradients. The TLR and PLR were estimated by elevation band as shown in Figure 3. The TLR and PLR are given as an input to set up the SWAT model for sub-catchment calculations of snowfall and snowmelt, as well as parameters in calibration. Figures 3a and 3b illustrate the TLR or inverse changes in temperature with altitude (Gardner et al., 2009). Figures 3a and 3b also show the winter and summer months' temperature variations in relation to elevation differences, as well as the inherent variation due to seasonal cycles at each sub-catchment. While winter temperatures in low-altitude portions of the catchment vary between 9^{o}C and 21^{o}C, summer temperatures range between 22^{o}C and 27^{o}C. At high altitudes, the largest temperature span (21^{o}C) occurs during winter months whereas the summer months' temperature span (5^{o}C) remains the same along the catchment. Parameter sensitivity in daily and monthly analyses (described in Table 3) evidenced SWAT's ability to simulate flows in response to snowmelt rather than changes in temperatures. Figure 3b evidences such sensitivity since the temperature between April and September remains within a 5^{o}C temperature span.

Figure 4 shows annual averages of snowpack variations by elevation band (10 numbers) computed at each sub-catchment for the 1991-2030 period. These variations are expressed in fractional snowpack at each sub-catchment, which at the same time define the variations in TLRs and PLRs. The distribution of the fractional snowpack varied throughout the catchment from upstream to downstream sub-catchments. Figures 4a to 4d are examples of high-altitude drainage areas characterized by high and variable snowpacks. In contrast, low-land variations upstream of Rampur station (Figures 4e and 4f) evidenced small variability and low values of accumulated snow. Downstream of Rampur (Figures 4g and 4h) illustrate slightly larger variations in snow accumulation with average values below 50 mm/year. Figure 5 is consistent with the fractional variations in snowpack expressed above, expanding such variations into multidecade contributions (1991-2000, 2001-2008, 2011-2020 and 2021-2030). In this figure, snowpack variation is highlighted at each catchment on a cumulative annual average. Figure 5 shows that sub-catchments at high elevations, such as SB1, SB2, SB3, SB8, SB15 and SB16, receive the highest amounts of snowpack. When compared intra-annually, the scenarios computed between 1991-2000 and 2001-2008 showed higher snowpack amounts than those calculated between 2011-2020 and 2021-2030. This difference in snowpack amount mainly occurred due to the variations in fractional snow covers.

Figures 6a-e show the spatial distribution of multidecadal averages of precipitation, snowpack, snowmelt, rainfall-runoff and total water yields (contributed by both snowmelt runoff and rainfall runoff) for the period 1991-2008 and their differences with respect to the near-term period 2011-2030. Figure 6a shows that the lower portion of the catchment (i.e., SB10, SB11, SB12 and SB13) and highest elevated part of the catchment (i.e., SB14, SB15 and SB16) had the largest precipitation (1991-2030). However, when compared with split time series sets, such as the 1991-2008 and 2011-2030 time series sets, precipitation decreases in the high elevation sub-catchments and increases in the lower parts. The snowpack and snowmelt plots have shown similar kinds of trends in their time series values. A decrease in the snowpack amounts can be observed in Figures 6b and 6c. Figure 6d also shows that the contribution of runoff (due to rainfall) has increased during the time 2011-2030. Figure 6e shows an increase in total water yield in subcatchments at low elevations. The portions of the watershed most vulnerable to hydrologic changes, specifically responses to variations in snow melting and snow accumulation, are the mid- to low-altitude portions of the catchment upstream of Rampur station.

Figure 7 illustrates the magnitude of change (shown as "% of change") in snowpack amount as a function of the fraction of elevation bands. The results showed a decrease in snowpack amount recorded from a minimum of 5% to a maximum of 42% across all the subcatchments. The subcatchments SB1, SB2, SB3 and SB8 correspond with the utmost decrease in snowpack amount (20% to 42%); whereas, the subcatchments SB5, SB7, SB14, SB15 and SB16 showed a small to moderate decrease in snowpack amount (4% to 20%). The above showed significant variations in the water balance components of the Satluj River catchment, illustrating an enormous change in snowpack amount over different sub-catchments.

5. Conclusion

This study analyzed the snowpack and snowmelt computations in high elevations of the Satluj River Himalayan catchment. In this study, the snowpack and snowmelt have been evaluated at multiple elevation bands, illustrating spatial variations in their amount at each subcatchment. For the computation of snowpack and snowmelt, both measured and GCM data sets were used to highlight the intraannual changes in snowmelt and snowpack. This study showed an enormous spatial and temporal variability in snowpack amount at elevation bands. The average TLR and PLR were used to compute the more accurate estimation of snowpack. For this, various model calibration parameters were considered and then sensitivity was analyzed. Based on the sensitivity analysis, significant sensitive and nonsensitive parameters were identified, which helped to improve the accuracy of the computation of snowpack and snowmelt. The other water balance components such as precipitation, water yield due to rainfall and water yield due to snowmelt were spatial studies. The long-term spatial comparison of these water balance components showed noticeable spatial variability from upstream subcatchments to downstream subcatchments. The percentage of change analysis clearly showed that snowpack is highly variable over the Satluj catchment and it could be more variable in the near-term period.

Acknowledgment

We sincerely thank the India-WRIS project (RRSC-W, Indian Space Research Organization, India) and Central Water Commission (New Delhi, India) for providing the necessary data to successfully complete this research. We also thank the Intergovernmental Panel on Climate Change (IPCC) for providing the necessary GCM data sets for analysis.

References

Abbaspour, K.C., Yang, J., Maximov, I., Siber, R., Bogner, K., Mieleitner, J., Zobrist, J. and Srinivasan, R.: Modelling hydrology and water quality in the pre-alpine/alpine Thur watershed using SWAT, J. of Hydrol., 333, 413-430. 2007.

Abbaspour, K.C.: SWAT-CUP4: SWAT calibration and uncertainty programs – A user manual. Swiss Federal Institute of Aquatic Science and Technology, Eawag, 2011.

Anderson, E.A.: A Point Energy and Mass Balance Model of a Snow Cover, *NOAA Technical Report NWS 19*, 150 pp, February 1976.

Arnold, J. G., Srinivasan, R., Muttiah, R.S. and Williams, J.R.: Large area hydrologic modeling and assessment – Part I: model development, J. Am. Water Resour. Assoc., 34(1), 73–89, 1998.

Beniston, M.: Is snow in the Alps receding or disappearing? WIREs Climate Change (Wiley Interdisciplinary Reviews/Climate Change), doi:10.1002/wcc.179, 2012.

Bhambri, R. and Bolch, T.: Glacier mapping: a review with special reference to the Indian Himalayas, Progress in Physical Geography, 33(5), 672-704, 2009.

Bolch, T., Kulkarni, A., Kääb, A., Huggel, C., Paul, F., Cogley, J.G., Frey, H., Kargel, J.S., Fujita, K., Scheel, M. and Bajracharya, S.: The state and fate of Himalayan glaciers, Science, 336(6079), 310-314, 2012.

Change, I. C.: The Physical Science Basis. Working Group I Contribution to the Fifth Assessment. Report of the Intergovernmental Panel on Climate Change, Cambridge, United Kingdom and New York, USA, 2013.

FAO.: The Digitized Soil Map of the World and Derived Soil Properties (Version 3.6) FAO Land and Water Digital Media Series 1, FAO, Rome, 2007.

Ferrant, S., Caballero, Y., Perrin, J., Gascoin, S., Dewandel, B., Aulong, S., Dazin, F., Ahmed, S. and Maréchal, J.C.: Projected impacts of climate change on farmers' extraction of groundwater from crystalline aquifers in South India, Scientific Reports, 4, 2014.

Ficklin, D. L. and Barnhart, B. L.: SWAT hydrologic model parameter uncertainty and its implications for hydroclimatic projections in snowmelt-dependent watersheds, J. of Hydrol., doi.org/10.1016/j. jhydrol.2014.09.082, 2014.

Fontaine, T. A., Cruickshank, T. S. and Arnold, J. G.: Development of a snowfall-snowmelt routine for mountainous terrain for the soil water assessment tool (SWAT), J. of Hydrol., 262, 209–223, 2002.

Gardner, A. S., Sharp, M. J., Koerner, R. M., Labine, C., Boon, S., Marshall, S. J. and Lewis, D.: Near-surface temperature lapse rates over Arctic glaciers and their implications for temperature downscaling, J. of Climate, 22(16), 4281-4298, 2009.

GLCF. Shuttle Radar Topography Mission (SRTM) Technical Guide, University of Maryland, USA, srtm.csi.cgiar.org, 2005.

IPCC: Climate change 2013: the physical science basis. In: Stocker TF, Qin D, Plattner GK, Tignor M, Allen SK, Boschung J, Nauels A, Xia Y, Bex V, Midgley PM (eds) Contribution of Working Group I to the Fifth Assessment Report of the Intergovernmental Panel on Climate Change. Cambridge University Press, Cambridge, United Kingdom and NY, USA, p 1535. doi:10.1017/CBO9781107415324, 2013.

Jain, S.K., Tyagi, J. and Singh, V.: Simulation of runoff and sediment yield for a Himalayan watershed using SWAT, J. Water Resour. Protect., 2, 267-281, 2010.

Legates, D. R. and McCabe Jr, G. J.: Evaluating the use of" goodness-of-fit" measures in hydrologic and hydroclimatic model validation, Water Resources Research, 35(1), 233-241, 1999.

Lu, G. Y. and Wong, D. W.: An adaptive inverse-distance weighting spatial interpolation technique, Computers & Geosciences, 34(9), 1044-1055, 2008.

Mahmood, R. and Babel, M.S.: Evaluation of SDSM developed by annual and monthly sub-models for downscaling temperature and precipitation in the Jhelum Catchment, Pakistan and India, Theor. Appl. Climatol., 113, 27-44. DOI: 10.1007/s00704-012-0765-0, 2012.

Mote, P. W., A. F. Hamlet, and D. P. Lettenmaier: Variability and trends in mountain snowpack in western North America. In Proceedings of the Western Snow Conference, April 19-22, 2004, Richmond, BC. K. Elder et al., eds., 15–22, 2005.

Mote, P. W.: Climate-driven variability and trends in mountain snowpack in western North America, J. Climate, 19, 6209–6220, 2006.

Narsimlu, B., Gosain, A.K. and Chahar, B.R.: Assessment of future climate change impacts on water resources of Upper Sind River Catchment, India, using SWAT Model, Water Resour. Manage. DOI: 10.1007/s11269-013-0371-7, 27: 3647–3662, 2013.

Neitsch, S. L., Arnold, J.G., Kiniri, J.R. and Williams, J.R.: Soil Water Assessment Tool Theoretical Documentation Version 9. Texas Water Resources Institute of Technical Report No. 406, Texas A & M University, 2011.

Neupane R. P., Yao J., White J. D.: Estimating the effects of climate change on the intensification of monsoonal-driven stream discharge in a Himalayan watershed. Hydrol Process 6250:6236–6250. doi:10.1002/hyp.10115, 2013.

Hydrol. Earth Syst. Sci. Discuss., doi:10.5194/hess-2016-689, 2017
Manuscript under review for journal Hydrol. Earth Syst. Sci.
Published: 9 January 2017

Hydrology and Earth System Sciences
Open Access
Discussions

Qiao, L., Pan, Z., Herrmann, R. and Hong, Y.: Hydrological variability and uncertainty of lower Missouri River Catchment under changing climate, J. of the American Water Resources Association (JAWRA), 1-15. DOI: 10.1111/jawr.12126, 2013.

Shrestha, B., Babel, M.S., Maskey, S., van Griensven, A., Uhlenbrook, S., Green, A. and Akkharath, I.: Impact of climate change on sediment yield in the Mekong River Catchment: a case study of the Nam Ou Catchment, Lao PD, Hydrol. and Earth Syst. Sci., 17(1), 1-20, 2013.

Singh, P., K.H. Umesh, and N. Kumar, 2008. Modelling and estimation of different components of streamflow for Gangotri Glacier basin, Himalayas. Hydrological Sciences Journal 53: 309-322.

Singh, V., Bankar, N., Salunkhe, S.S., Bera, A.K. and Sharma, J.R.: Hydrological streamflow modeling on Tungabhadra catchment: parameterization and uncertainty analysis using SWAT CUP, Current Science, 104(9), 1187-1199, 2013.

Singh, V. and Goyal, M. K.: Analysis and trends of precipitation lapse rate and extreme indices over north Sikkim eastern Himalayas under CMIP5ESM-2M RCPs experiments, Atmospheric Research, 167, 34-60, 2016a.

Singh, V. and Goyal, M.K.: Changes in climate extremes by the use of CMIP5 coupled climate models over eastern Himalayas, Environmental Earth Sciences, 75(9), 1-27, 2016b.

Singh S, Kumar R, Bhardwaj A, Sam L, Shekhar M, Singh A, Kumar R and Gupta A.: Changing climate and glacio-hydrology in Indian Himalayan Region: a review. Wiley Interdiscip Rev Clim Change 7(3):393–410. doi:10.1002/wcc.39, 2016.

Snell, S. E., Gopal, S. and Kaufmann, R. K.: Spatial interpolation of surface air temperatures using artificial neural networks: Evaluating their use for downscaling GCMs, J. of Climate, 13(5), 886-895, 2000.

Sridhar, V. and Nayak, A.: Implications of climate-driven variability and trends for the hydrologic assessment of the Reynolds Creek Experimental Watershed Idaho, J. of Hydrol., 385, 183–202, 2010.

Taylor, K. E., Stouffer, R. J. and Meehl, G. A.: An overview of CMIP5 and the experiment design, Bulletin of the American Meteorological Society, 93(4), 485-498, 2012.

Thornton, P.K., Van de Steeg, J., Notenbaert, A. and Herrero, M.: The impacts of climate change on livestock and livestock systems in developing countries: A review of what we know and what we need to know, Agricultural Systems, 101(3), 113–127. DOI:10.1016/j.agsy.2009.05.002, 2009.

Xu, Y., Ramanathan, V. and Washington, W.M.: Observed high-altitude warming and snow cover retreat over Tibet and the Himalayas enhanced by black carbon aerosols, Atmospheric Chemistry and Physics, 16(3), 1303-1315, 2016.

Yang, J., Reichert, P., Abbaspour, K.C. and Yang, H.: Hydrological modelling of the Chaohe Catchment in China: Statistical model formulation and Bayesian inference, J. of Hydrol., 340 (3–4), 167–182, 2007.

Zhou, J., Liu, Y., Guo, H. and He, D.: Combining the SWAT model with sequential uncertainty fitting algorithm for streamflow prediction and uncertainty analysis for the Lake Dianchi Catchment, China, Hydrological Processes, 28(3), 521-533, 2014.

Hydrol. Earth Syst. Sci. Discuss., doi:10.5194/hess-2016-689, 2017
Manuscript under review for journal Hydrol. Earth Syst. Sci.
Published: 9 January 2017

Tables

Table 1: Details of water balance components simulated in the SWAT model

Model Simulation Details	
General details	Satluj catchment
Simulation period (years)	16
Warmup (years)	3
Hydrological response units	358
Sub-catchments	16
Output time step	Daily, Monthly
Watershed area (km^2)	51055
Water Balance Ratios	
Streamflow/precipitation	0.63
Baseflow/total flow	0.25
Surface runoff/total flow	0.45
Percolation/precipitation	0.26
Deep recharge/precipitation	0.01
ET/precipitation	0.36
Water Balance Components (mm)	
ET	382.0
Precipitation	1073.5
Surface runoff	304.8
Lateral flow	113.0
Return flow	259.0
Percolation to shallow aquifer	283.4
Revaporation from shallow aquifer	10.2
Recharge to deep aquifer	14.2

Hydrol. Earth Syst. Sci. Discuss., doi:10.5194/hess-2016-689, 2017
Manuscript under review for journal Hydrol. Earth Syst. Sci.
Published: 9 January 2017

Table 2: Description of model calibration parameters

Streamflow parameters selected for calibration and validation	Description
SNOCOVMX.bsn	Minimum snow water content
HRU_SLP.hru	Average slope steepness
SOL_K.sol	Soil hydraulic conductivity
SNO50COV.bsn	Fraction of snow volume
PLAPS.sub	Precipitation lapse rate
SFTMP.bsn	Snowfall temperature
GWQMN.gw	Threshold depth of water in shallow aquifer required for return flow
CH_N2.rte	Manning roughness coefficient for main channel
SOL_BD.sol	Moist bulk density
SOL_AWC.sol	Available water capacity of the soil layer
GW_REVAP.gw	Groundwater "revaporation" coefficient
SMTMP.bsn	Snowmelt base temperature
ALPHA_BF.gw	Baseflow alfa factor coefficient
SMFMN.bsn	Melt factor for snow on December 21^{st}
SOL_Z.sol	Depth from soil surface to bottom layer
GW_DELAY.gw	Groundwater delay time
TLAPS.sub	Temperature lapse rate
CH_K2.rte	Effective hydraulic conductivity
SMFMX.bsn	Melt factor for snow on June 21^{st}
CN2.mgt	Curve number coefficient

Hydrol. Earth Syst. Sci. Discuss., doi:10.5194/hess-2016-689, 2017
Manuscript under review for journal Hydrol. Earth Syst. Sci.
Published: 9 January 2017

Hydrology and Earth System Sciences Discussions
Open Access

557 Table 3: Aggregate parameters and their values, ranges and global sensitivity results

			Daily			
SI. No.	Parameter	Fitted Value	Minimum Value	Maximum Value	t-Stat	P-Value
1	A__SNOCOVMX.bsn	300.0	0.0	500.0	-2.1	0.03
2	R__HRU_SLP.hru	0.2	0.2	0.2	-0.2	0.9
3	R__SOL_K.sol	0.3	0.0	1.3	-0.2	0.8
4	R__SNO50COV.bsn	0.4	0.0	50.0	-0.2	0.8
5	A__PLAPS.sub	277.0	100.0	300.0	0.3	0.8
6	A__SFTMP.bsn	-1.7	-1.8	1.0	-0.4	0.7
7	V__GWQMN.gw	1.0	0.8	1.1	-0.4	0.7
8	V__CH_N2.rte	0.3	0.2	0.3	0.5	0.6
9	R__SOL_BD.sol	1.4	1.2	1.5	0.7	0.5
10	R__SOL_AWC.sol	0.6	0.6	0.7	0.7	0.5
11	V__GW_REVAP.gw	0.0	0.0	0.0	0.9	0.4
12	R__SMTMP.bsn	-0.5	-2.7	2.0	-0.9	0.4
13	A__ALPHA_BF.gw	0.12	0.06	0.2	-1.4	0.2
14	R__SMFMN.bsn	7.4	6.4	7.7	-1.4	0.2
15	R__SOL_Z.sol	2813	100	4000.0	1.6	0.1
16	V__GW_DELAY.gw	10.5	-88.6	50.1	-2.1	0.02

17	A__TLAPS.sub	-4.1	-7.0	2.5	-2.2	0.01
18	V__CH_K2.rte	27	22	75.0	2.4	0.0
19	R__SMFMX.bsn	0.5	-0.5	1.4	6.4	0.0
20	R__CN2.mgt	0.03	0.0	0.1	-8.6	0.0
			Monthly			
1	R__SOL_BD.sol	1.0	0.9	1.6	-0.1	0.9
2	R__SMFMN.bsn	9.1	6.2	11.2	0.3	0.8
3	A__PLAPS.sub	337	100	350.0	-0.3	0.7
4	V__GW_REVAP.gw	0.1	0.1	0.2	-0.4	0.7
5	R__TLAPS.sub	-4.6	-6.2	2.5	0.4	0.7
6	V__GWQMN.gw	1.6	0.8	1.7	0.7	0.5
7	R__SOL_AWC.sol	0.5	0.5	0.9	-0.8	0.4
8	R__SOL_Z.sol	1296	1265	4388.0	-0.8	0.4
9	V__ALPHA_BF.gw	0.11	0.0	1.7	0.8	0.4
10	R__SNOCOVMX.bsn	100	50	500.0	-1.0	0.3
11	R__SMTMP.bsn	0.7	0.6	1.7	1.1	0.3
12	R__SFTMP.bsn	1.4	1.0	1.9	1.4	0.2
13	R__SMFMX.bsn	0.4	0.3	1.5	-1.8	0.1

Hydrol. Earth Syst. Sci. Discuss., doi:10.5194/hess-2016-689, 2017
Manuscript under review for journal Hydrol. Earth Syst. Sci.
Published: 9 January 2017

14	R__SOL_K.sol	0.5	0.6	1.3	2.1	0.0
15	V__GW_DELAY.gw	20	-70	251	2.6	0.0
16	R__CN2.mgt	0.02	0.0	0.1	-4.6	0.0
17	R__SNO50COV.bsn	0.2	0.0	1.0	-11.7	0.0

Table 4: Model calibration and validation results using the SUFI method for the daily and monthly analysis

Outlet Station	Calibration (1991 - 2000)					
	Daily			Monthly		
	p-factor	r-factor	R^2	p-factor	r-factor	R^2
Rampur	0.46	1.89	0.75	0.41	1.90	0.71
Kasol	0.57	1.50	0.76	0.57	1.57	0.78
Suni	0.52	1.60	0.72	0.49	1.43	0.73
Outlet Station	Validation (2001 - 2008)					
	Daily			Monthly		
	p-factor	r-factor	R^2	p-factor	r-factor	R^2
Rampur	0.43	1.89	0.62	0.45	1.92	0.65
Kasol	0.52	1.67	0.71	0.60	1.62	0.73
Suni	0.52	1.72	0.65	0.58	1.52	0.71

Hydrol. Earth Syst. Sci. Discuss., doi:10.5194/hess-2016-689, 2017
Manuscript under review for journal Hydrol. Earth Syst. Sci.
Published: 9 January 2017

Hydrology and Earth System Sciences
Open Access
Discussions

Figure Captions

Fig. 1: Study area map of Satluj river catchment (up to Kasol station/gauge).

Fig. 2: Sub-catchment and annual variability in snowpack and snowmelt (annual average) for the year 1991 to 2008.

Fig. 3: Distribution of average temperature over the sub-watershed's centroid elevation (in chronological order); (a) winter season and (b) summer season.

Figure 4: (a-h) Sub-catchment snowpack variability (average annual) based on the fractional elevation bands in long term climate domain (1991-2030) and (b) Cumulative variability in snowpack amount over different sub-catchments of Satluj catchment in different temporal domains.

Figure 5: Cumulative variability in snowpack amount over different sub-catchments of Satluj catchment in different temporal domains.

Fig. 6: Historical average (1991-2008) and differences between near-term and historical average for (a and b) precipitation, (c and d) snowpack/snowfall, (e and f) snowmelt, (g and h) water yield (due to snow) and (I and j) total water yield (snowmelt and rainfall runoff) in the Satluj River Basin.

Fig. 7: Percentage of change in snowpack amount (average annual) over different sub-catchments of Satluj River.

Hydrol. Earth Syst. Sci. Discuss., doi:10.5194/hess-2016-689, 2017
Manuscript under review for journal Hydrol. Earth Syst. Sci.
Published: 9 January 2017

Hydrology and Earth System Sciences
Discussions
Open Access

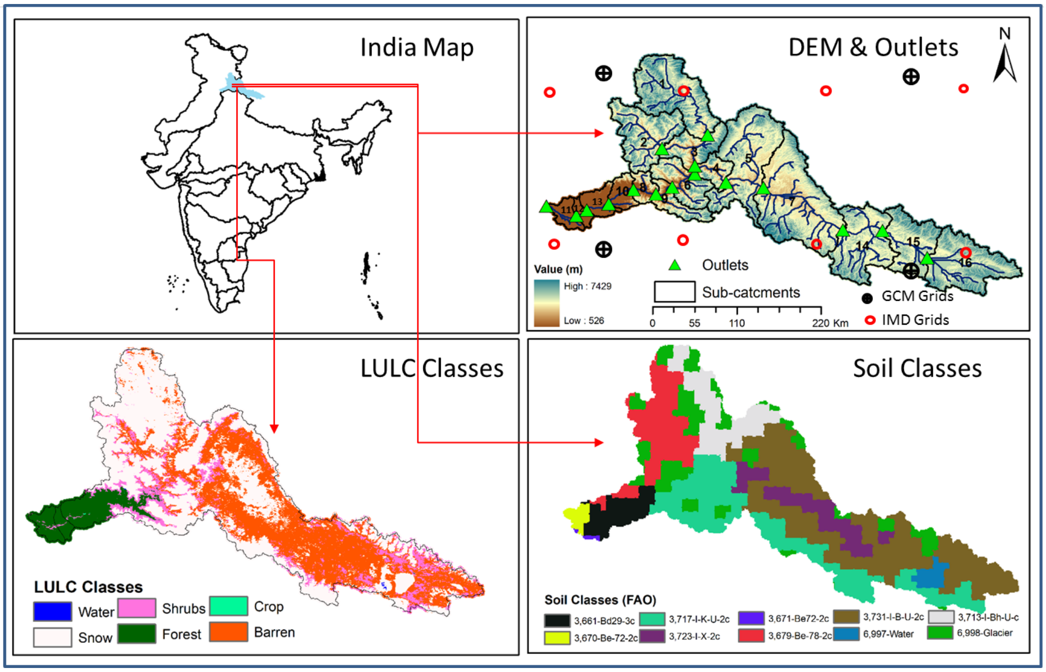

Fig. 1: Study area map of Satluj river catchment (up to Kasol station/gauge).

Hydrol. Earth Syst. Sci. Discuss., doi:10.5194/hess-2016-689, 2017
Manuscript under review for journal Hydrol. Earth Syst. Sci.
Published: 9 January 2017

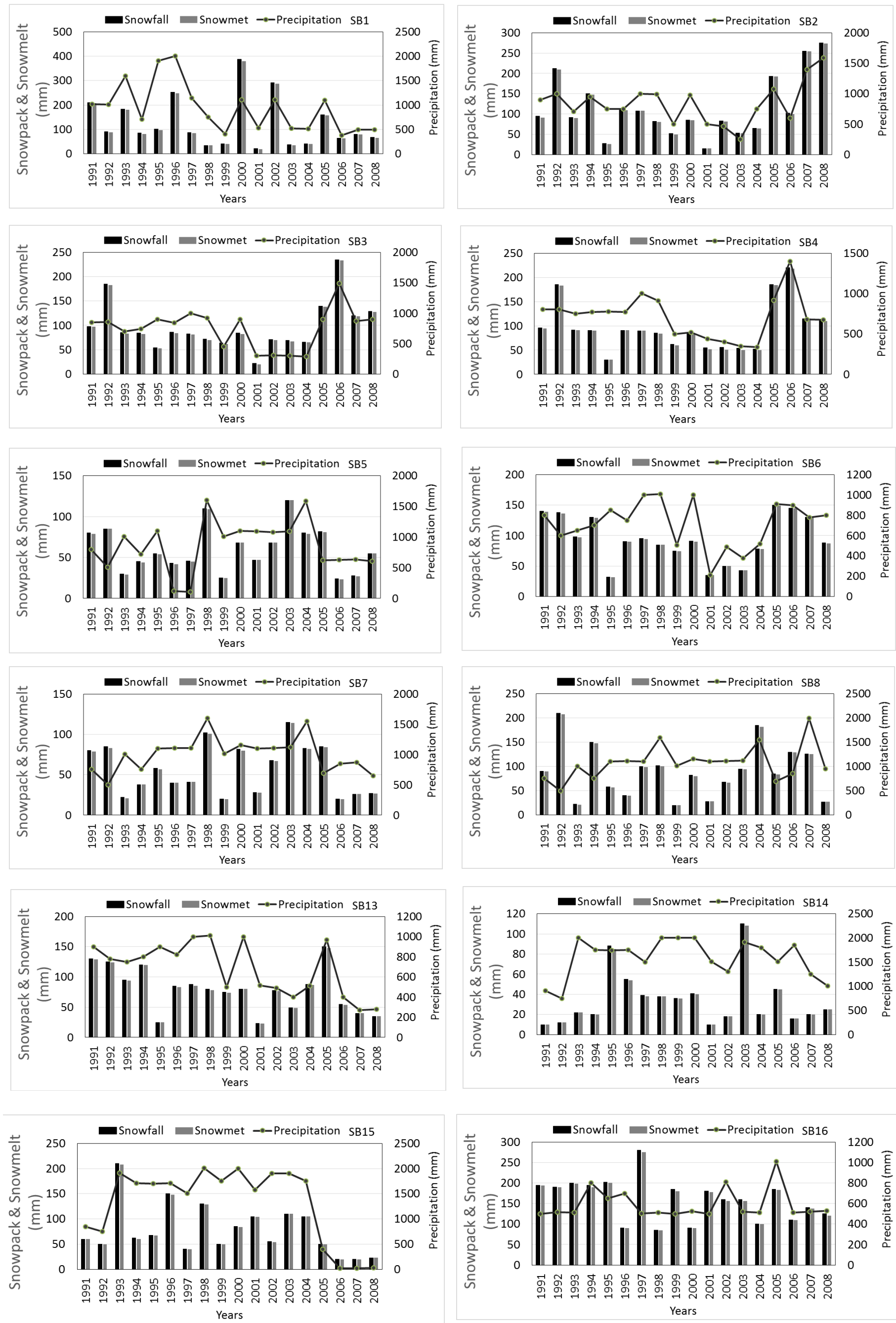

Fig. 2: Sub-catchment and annual variability in snowpack and snowmelt (annual average) for the year 1991 to 2008.

(a)

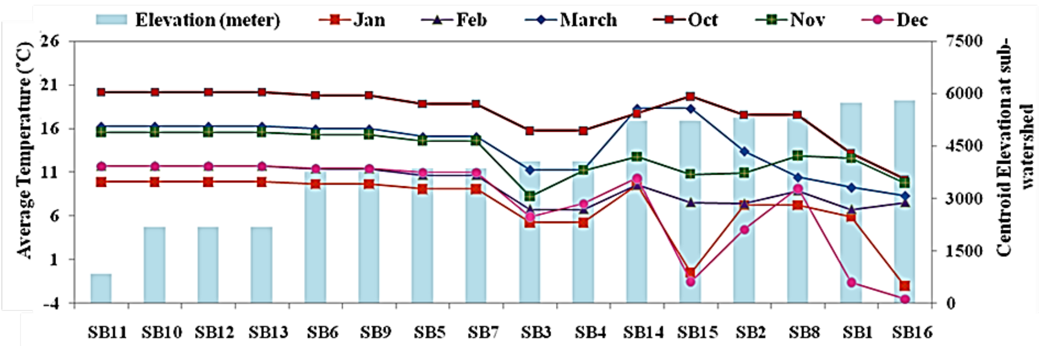

(b)

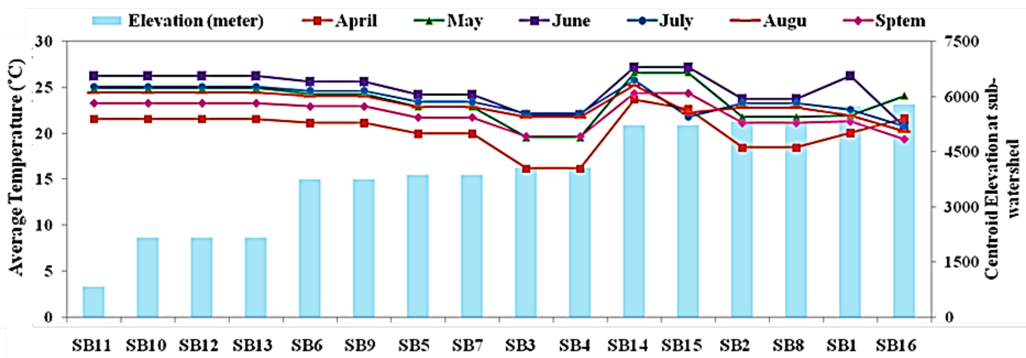

Fig. 3: Distribution of average temperature over the sub-watershed's centroid elevation (in chronological order); (a) winter season and (b) summer season.

Hydrol. Earth Syst. Sci. Discuss., doi:10.5194/hess-2016-689, 2017
Manuscript under review for journal Hydrol. Earth Syst. Sci.
Published: 9 January 2017

Hydrology and Earth System Sciences Discussions

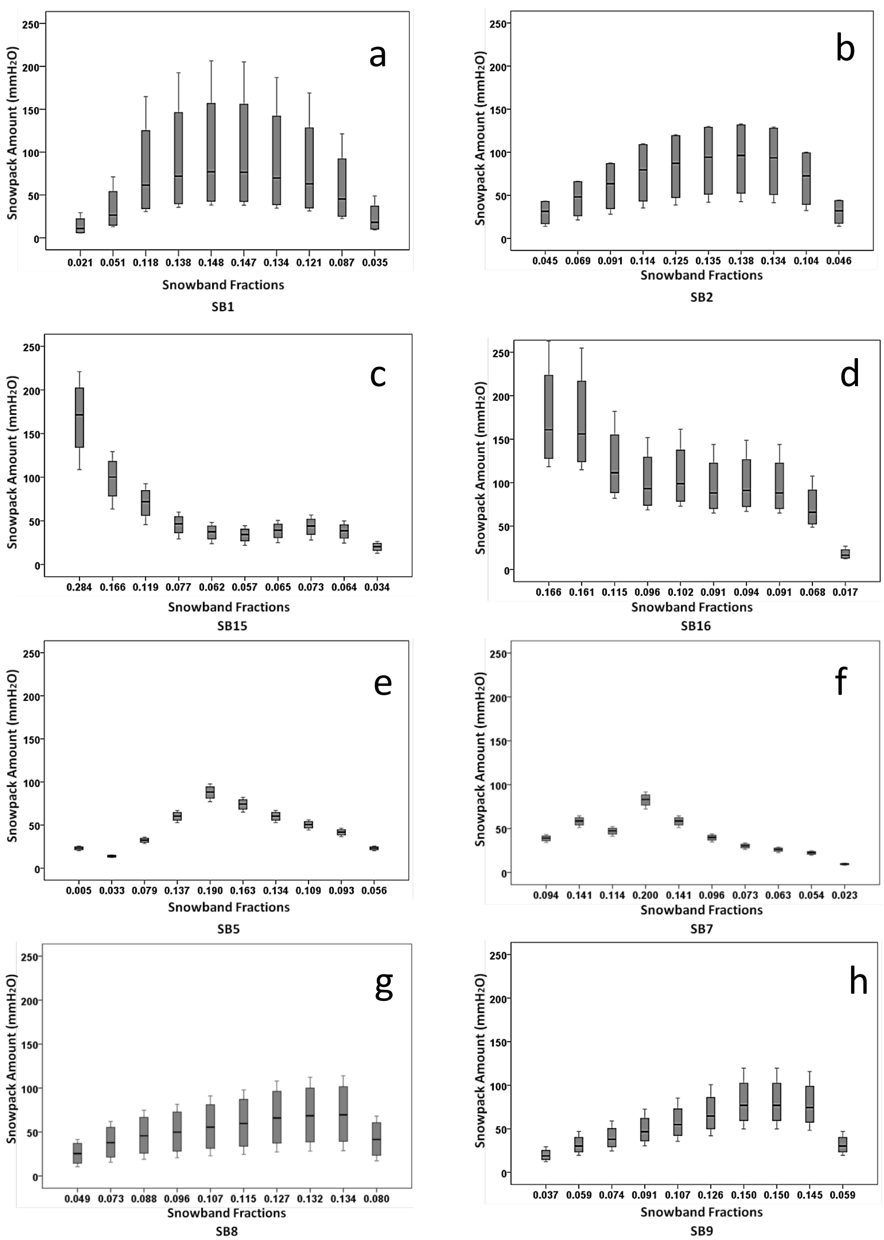

Figure 4: (a-h) Sub-catchment snowpack variability (average annual) based on the fractional elevation bands in long term climate domain (1991-2030) and (b) Cumulative variability in snowpack amount over different sub-catchments of Satluj catchment in different temporal domains.

Hydrology and Earth System Sciences Discussions

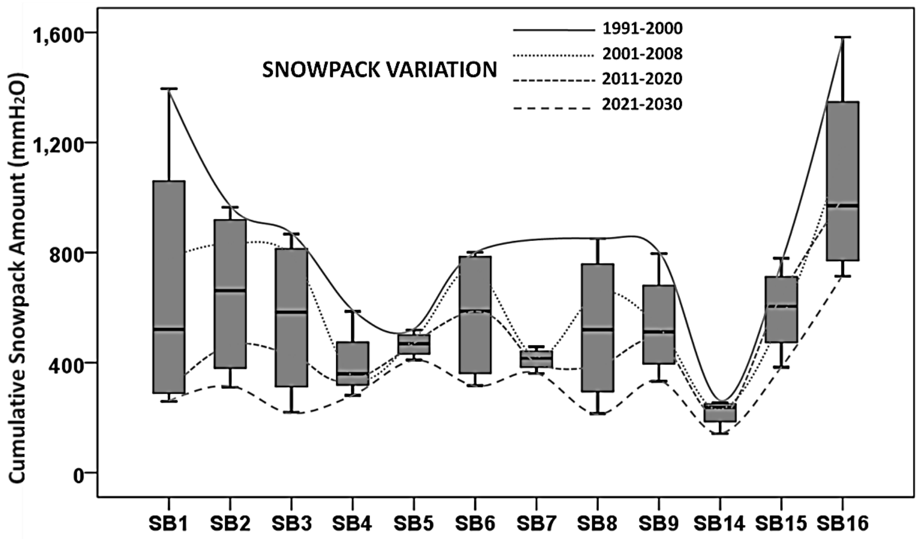

Figure 5: Cumulative variability in snowpack amount over different sub-catchments of Satluj catchment in different temporal domains.

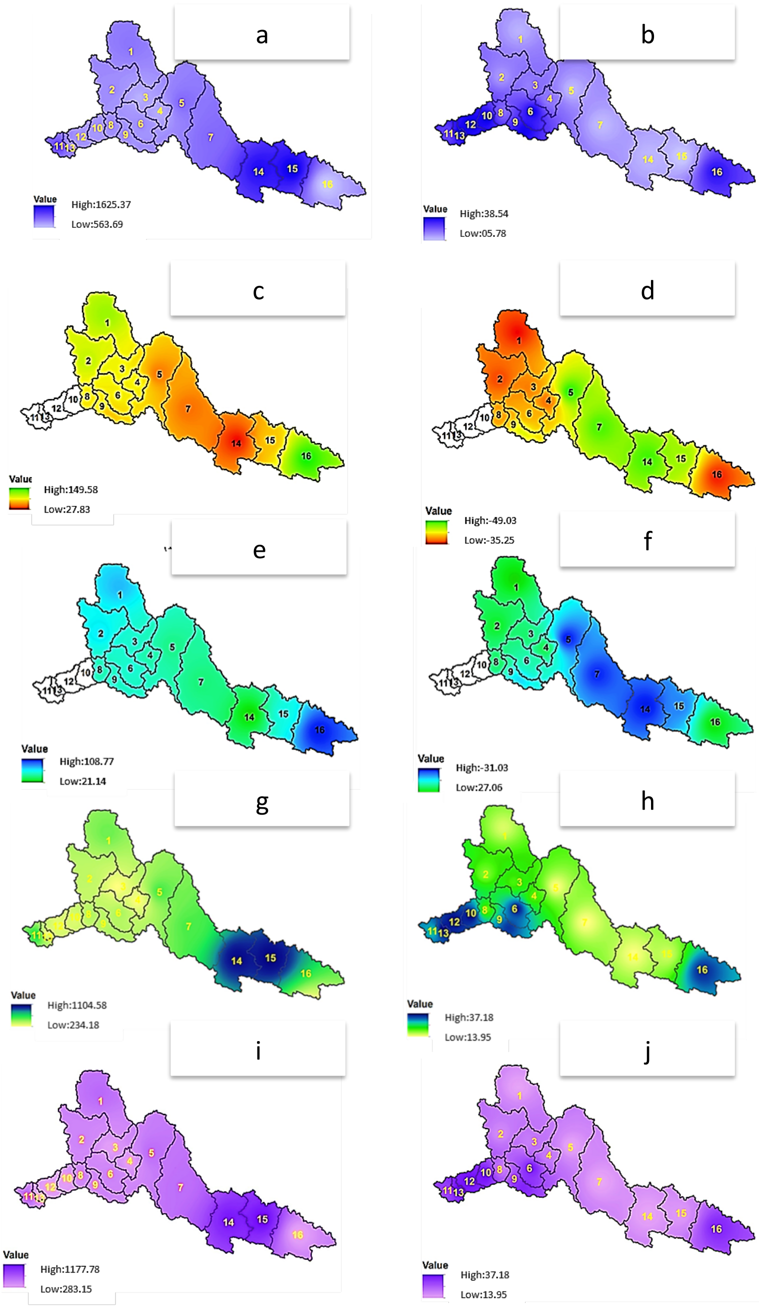

Fig. 6: Historical average (1991-2008) and differences between near-term and historical average for (a and b) precipitation, (c and d) snowpack/snowfall, (e and f) snowmelt, (g and h) water yield (due to snow) and (I and j) total water yield (snowmelt and rainfall runoff) in the Satluj River Basin.

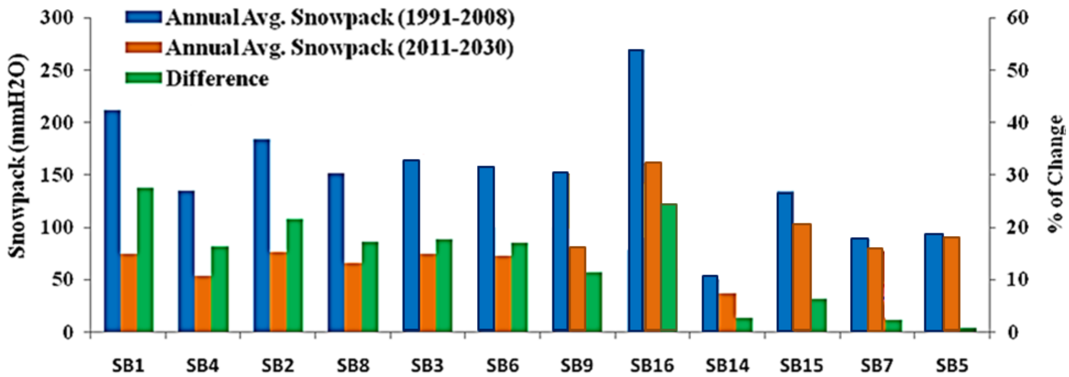

Fig. 7: Percentage of change in snowpack amount (average annual) over different sub-catchments of Satluj River.